East European Journal of Physics. 3. 168-179 (2025)
DOI:10.26565/2312-4334-2025-3-15 ISSN 2312-4334

THE STAGNATION POINT FLOW OF THE MHD CASSON POLYMERIC NANOFLUID FLOWS TOWARD A WAVY CIRCULAR CYLINDER SATURATED WITH A POROUS MEDIUM UNDER CONVECTIVE NIELD CONDITIONS AND THERMAL RADIATION

P. Venkata Subrahmanyam[a], Gandrakota Kathyayani[a]*, Gattu Venkata Ramudu[a], K. Venkatadri[b]
[a]*Department of Applied Mathematics, Yogi Vemana University, Kadapa, A.P., India*
[b]*Department of Mathematics, Mohan Babu University (Erstwhile Sree Vidyanikethan Eng. Coll.), Tirupati A.P-517 102, India*
[*]*Corresponding Author E-mail: kathyagk@yvu.edu.in*
Received May 3, 2025; revised June 19, 2025; accepted June 24, 2025

This study conducts a thorough numerical investigation employing the bvp4c technique to delve into the stagnation-point flow of a magnetohydrodynamic (MHD) Casson polymeric nanofluid around a wavy circular porous cylinder. It takes into account activation energy and thermal radiation, emphasizing the significant impact of thermal radiation on fluid flow, concentration and temperature profiles. The effects of thermal radiation within the energy equation are carefully considered, along with convective Nield boundary conditions, enabling a comprehensive analysis. By introducing dimensionless variables, the study transforms the partial differential equation into ordinary equations, facilitating the application of the shooting scheme to approximate the solution. The meticulously examined results offer detailed insights into temperature, velocity and mass concentration profiles, highlighting the profound influence of thermal radiation on these parameters. Furthermore, a comprehensive graphical presentation of each engineering parameter is provided, offering a nuanced understanding of the intricate physical phenomena involved, with particular attention to the influence of thermal radiation.
Keywords: *Stagnation-point flow; Thermal radiation; Casson polymeric nanofluid; bvp4c technique; Magnetohydrodynamic (MHD)*
PACS: 47.70.Fw, 44.20.+b, 44.25.+f, 47.10.ad, 47.15.Cb

1. INTRODUCTION

Casson fluids, which are non-Newtonian and possess yield stress, have emerged as valuable models for studying the flow of complex fluids in a wide range of industrial and biological systems. When magnetic fields are introduced to such systems, the effects can be quite complex due to their potential to alter the fluid dynamics and heat transfer characteristics. The present study, therefore, aims to investigate the interplay between MHD effects, Casson rheology, and nanoparticle dispersion in the context of stagnation point flow. Stagnation point flow is a critical phenomenon that occurs when a fluid is brought to rest by an external object. It has been extensively studied in the past, and it is known that the rheological properties of the fluid play a critical role in determining flow behaviour. When magnetic fields are present, the fluid dynamics can be further modified, leading to a more complex flow behaviour. Moreover, if nanoparticles are present in the fluid, their dispersion can also be affected by the magnetic field, leading to further modifications in the fluid behaviour. Thus, this study intends to examine the impact of MHD consequences, Casson rheology, and nanoparticle dispersion on stagnation point flow. The research findings will provide insights into the complex behaviour of Casson fluids under the impact of magnetic fields. They will help in designing better models for predicting the flow of complex fluids in various industrial and biological systems.

The study of Magnetohydrodynamic (MHD) Casson nanofluid flow around a cylinder that is saturated with a porous medium has gained significant attention in recent research. This phenomenon is complex and intriguing due to the interaction of MHD effects, porous medium, and nanofluid dynamics. Various numerical and analytical studies have been conducted to investigate this phenomenon. For instance, Alwawi et al. [3] delve into the characteristics of the magnetohydrodynamic (MHD) convection flow of Casson nanofluid with a shrinking sheet. The researchers used the Runge-Kutta method to perform their investigation while taking into account the effects of suction/injection on the wall. Narender et al. [5] investigated the behaviour of a fluid flow over a surface that is being stretched non-linearly. The fluid used was a type of nanofluid called the Casson nanofluid, which exhibits unique properties due to the presence of nanoparticles. The study also considered the effects of velocity and convective boundary conditions, which are important factors that can significantly influence the behaviour of the fluid. Thamaraikannan et al. [19] studied the effects of periodic body acceleration and thermal radiation on pulsating MHD Casson nanofluid flow through a porous channel. Their research sheds light on the behaviour of MHD Casson nanofluid flows under various scenarios, providing valuable insights for researchers in the field. The impact of a porous medium on the flow of MHD Casson nanofluid was examined in a recent study [12]. The study aims to examine mass and heat transfers of MHD Casson nanofluids flowing through porous media past a stretching sheet. The researchers also considered the impact of Newtonian heating and chemical reactions on the flow. By using mathematical models and simulations, the study found that the existence of a porous medium significantly affects the flow behaviour of MHD Casson nanofluid. Furthermore, the investigation carried out by Bosli et al. [4] thoroughly examined the natural convection flow and heat transfer of a Casson nanofluid flowing past a vertical plate under convective boundary conditions, while being aligned with MHD. The results of this study shed light

Cite as: P.V. Subrahmanyam, G. Kathyayani, G.V. Ramudu, K Venkatadri, East Eur. J. Phys. 3, 168 (2025), https://doi.org/10.26565/2312-4334-2025-3-15

on the complex relationship between the dynamics of MHD Casson nanofluid and the effects of a porous medium. In recent research, there has been a focus on analyzing the behavior of Casson nanofluids in various flow scenarios. Researchers [17] looked into the numerical analysis of a three-dimensional Casson nanofluid magnetohydrodynamic (MHD) flow past an exponentially-stretching sheet.

The three-dimensional aspects of MHD Casson nanofluid flows were explored, revealing insights into the behaviour of these fluids in complex flow scenarios. On unstable MHD mixed convection flows of non-Newtonian Casson nanofluids, Gnanaprasanna & Singh [9] conducted another study on the stagnation zone of sphere-spinning impulsive fluids. This research contributed to the understanding of unsteady MHD effects on Casson nanofluid flows, particularly in the context of non-Newtonian fluids. These findings could be useful in designing more efficient and effective fluid systems in various industrial and scientific applications. The references cited in the text provide valuable information not only on MHD Casson nanofluid flows but also on related topics such as flow around cylinders and porous medium dynamics. For instance, Baig et al. [13] conducted a study that illuminates the effects of nanofluids in porous media by using thermal analysis to examine an Al_2O_3-Water nanofluid flow in a composite microchannel.

By adding nanoparticles to the base fluid, nanofluids have shown potential for enhancing heat transfer rates compared to traditional fluids. Kathyayani et al. [10] investigated nanofluid flow Stagnation-Point MHD flow Past 3-D Sinusoidal Cylinder with Brownian Motion and Thermophoresis Effects. Wang et al. [25] investigated mass transfer and natural convection heat using thermal radiation in a cavity that was partially filled with a porous material that was hygroscopic, which gives us insights into the heat and moisture transfer phenomena in porous media. One of the well-known models for modelling nanofluid hydrothermal characteristics is Buongiorno's [8] two-component nanoscale model, which includes both conservation of energy and nanoparticle diffusion (mass transfer) equations. This formulation has been very successfully applied for investigating enhanced heat transfer in nanofluids and emphasises thermophoresis and random diffusion (Brownian motion) as the dominant mechanisms. Several researchers have conducted investigations on buoyancy-driven convective flow in a closed regime filled with Buongiorno nanofluids to explore the heat transfer performance in various geometrical shapes using a wide range of computational techniques. A study by Rana et al. [20] explored the analysis of alumina and titania-water nanofluid flow using theoretical and computational methods. The study investigated the impact of velocity slip, thermal slip, and Stefan blowing at the boundary of a horizontal stretching sheet, also known as the wall. The viscosity and thermal conductivity were calculated using the Pak-Cho model in combination with the non-homogeneous Buongiorno nanofluid model. The model has been extensively utilized since its inception. Akram et al. [7], [22] and The Buongiorno model was utilised by researchers Tripathi et al. [2], [11], [15],[16] in a study of nanofluids, which yielded significant accomplishments. The use of the Buongiorno model and Cattaneo-Christov double diffusion has been quite popular among researchers [14], [18], [21],[23] over the years for studying the heat and mass transmission of fluids.

The research field of Casson nanofluid has yet to explore the evaluation of its impact on a sinusoidal cylinder using a two-phase nanofluid model. Our work is distinctive in that it examines the effects of both Neild's conditions, which are taken to be exponential and Casson nanofluid convectional flow over a sinusoidal cylinder. The controlled PDEs used in our research are ODEs, which are subsequently solved computationally with MATLAB software's bvp4c and the shooting approach. The present method has the potential to address several environmental, pharmaceutical, and biological problems. This study has the potential to contribute to a better understanding of various fields and provide solutions to numerous challenges.

2. MATHEMATICAL MODEL

A steady stagnation-point flow incompressible Casson nanofluid was considered towards a wavy cylinder (Fig. 1). At each extreme radius of the cylinder's radius there were points of stagnation (points A, B, and C). The equation $x = \delta y^{1/c}$ can be used to characterise the streamlines, where c is a fraction of the stream velocities slope and stated as $c = b/a$ with $0 < c < 1$ called nodal point or with $-1 < c < 0$ called saddle point and c=0 refers to plane flow, δ is constant, provides a particular streamline. In the cylinder, points of minimum and maximum stagnation can be observed at positions B, A, and C. The velocity profiles of fluid flow particles in the x, y, and z-directions were taken into consideration with u, v and w respectively. In the Cartesian coordinate system Oxyz, the stagnation point is located at the system's origin, and the velocity profiles are expressed as

$$u_e = ax,\ \ v_e = aby,\ \ w_e = -(a+b)z\,. \tag{1}$$

In the stress-strain relation, the constitutive equation for a Casson fluid is as follows:

$$\tau^{\frac{1}{2}} = \tau_0^{\frac{1}{2}} + \mu\dot{\gamma}^{\frac{1}{2}}$$

$$\tau_{ij} = \begin{cases} 2(\mu_B + \dfrac{P_y}{\sqrt{2\pi}})e_{ij}\,, & \pi > \pi_c \\ 2(\mu_B + \dfrac{P_y}{\sqrt{2\pi_c}})e_{ij}\,, & \pi_c > \pi \end{cases} \tag{2}$$

A sinusoidal cylinder's boundary layer can be modelled by applying the following equations to represent the cylinder's boundary layer by the assumptions suggested above and using the Bernoulli equation, the pressure is removed, to model the sinusoidal cylinder's boundary layer by incorporating the Casson rheological effect term from Eq. (2) (sec [14, 18,24]).

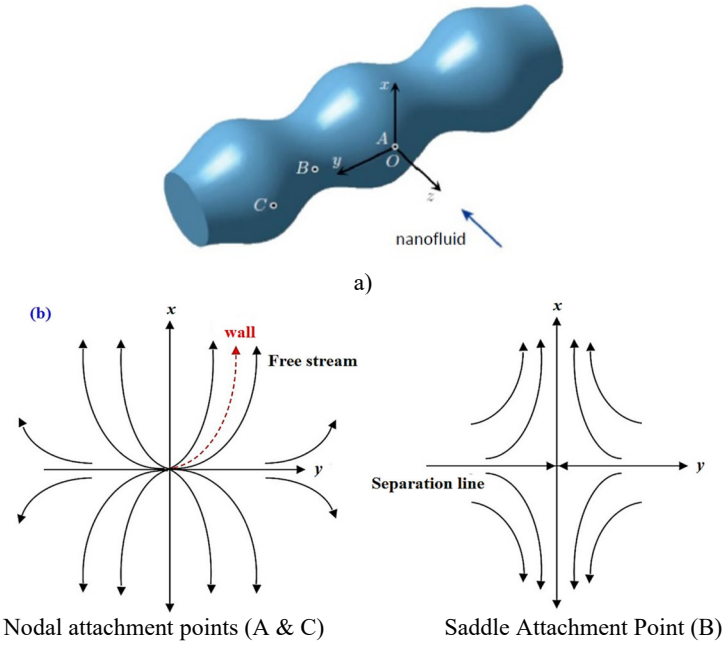

Figure 1. Schematic model and the streamlines

$$\frac{\partial u}{\partial x}+\frac{\partial v}{\partial y}+\frac{\partial w}{\partial z}=0 \tag{3}$$

$$u\frac{\partial u}{\partial x}+v\frac{\partial u}{\partial y}+w\frac{\partial u}{\partial z}=a^2x+\upsilon\left(1+\frac{1}{\beta}\right)\frac{\partial^2 u}{\partial z^2}-\frac{\sigma B_0^2}{\rho}(u-ax)-\frac{\upsilon}{\kappa}(u-ax) \tag{4}$$

$$u\frac{\partial v}{\partial x}+v\frac{\partial v}{\partial y}+w\frac{\partial v}{\partial z}=b^2y+\upsilon\left(1+\frac{1}{\beta}\right)\frac{\partial^2 v}{\partial z^2}-\frac{\sigma B_0^2}{\rho}(v-by)-\frac{\upsilon}{\kappa}(v-by) \tag{5}$$

$$u\frac{\partial T}{\partial x}+v\frac{\partial T}{\partial y}+w\frac{\partial T}{\partial z}=\left(\alpha+\frac{16\sigma_s T_\infty^3}{3k^*\left(\rho c_p\right)}\right)\frac{\partial^2 T}{\partial z^2}+\tau\left[D_B\frac{\partial T}{\partial z}\frac{\partial C}{\partial z}+\frac{D_T}{T_\infty}\left(\frac{\partial T}{\partial z}\right)^2\right] \tag{6}$$

$$u\frac{\partial C}{\partial x}+v\frac{\partial C}{\partial y}+w\frac{\partial C}{\partial z}=D_m\frac{\partial^2 C}{\partial z^2}+\frac{D_T}{T_\infty}\frac{\partial^2 T}{\partial z^2}-K_c^2\left(\frac{T}{T_\infty}\right)^n e^{-\frac{E_a}{K_0 T}}(C-C_\infty) \tag{7}$$

It also noticeable term in the equation (7), that the Arrhenius term is $K_c{}^2(C-C_\infty)\left(\frac{T}{T_\infty}\right)^n exp\left(-\left(\frac{E_a}{K_0 T}\right)\right)$.

The first-order chemical reaction rate was represented by K_c, When K_c is more than 0, a destructive reactant is produced. These boundary conditions lead to the following formula:

$$\begin{aligned} &u=v=w=0,\ -\kappa T_z=h_f\left(T_f-T\right),\ D_B C_z+\frac{D_T}{T_\infty}T_z=0 \qquad at \quad z=0\\ &u\to u_e, v\to v_e, T\to T_\infty, C\to C_\infty \qquad as \quad z\to\infty \end{aligned} \tag{8}$$

Each of the following equations has a similarity solution

$$\begin{aligned} &u=axf'(\eta),\ v=byg'(\eta),\ \ w=-\sqrt{a\upsilon}\left(f(\eta)+cg(\eta)\right),\ \frac{T-T_\infty}{T_w-T_\infty}=\theta(\eta)\\ &\phi(n)=\frac{C-C_\infty}{C_w-C_\infty},\ \eta=z\sqrt{\frac{a}{\upsilon}}, \end{aligned} \tag{9}$$

Notably, the derivative with respect to η indicates primes. The differential equations (3)-(7) converted to ODEs, which are nonlinear in nature, with the help of similarity transformations (9)

$$\left(1+\frac{1}{\beta}\right)f'''+\left(f+cg\right)f''-\left(f'\right)^2+1-M\left(f'-1\right)-\lambda\left(f'-1\right)=0 \tag{10}$$

$$\left(1+\frac{1}{\beta}\right)g'''+\left(f+cg\right)g''-c\left(g'\right)^2+c-M\left(g'-1\right)-\lambda\left(g'-1\right)=0 \tag{11}$$

$$\left(1+\frac{4}{3}Rd\right)\frac{1}{\mathrm{Pr}}\theta''+\left(f+cg\right)\theta'+Nb\,\theta'\phi'+Nt\left(\theta'\right)^2=0 \tag{12}$$

$$\phi''+Sc\left(f+g\right)\phi'+\frac{Nt}{Nb}\theta''-Sc\,\sigma\,\left(1+\delta\theta\right)^n\exp\left(\frac{-E}{1+\delta\theta}\right)\phi=0 \tag{13}$$

The modified boundary conditions are

$$\begin{aligned} &f=0, f'=0, g=0, g'=0, \theta'=-Bi\left(1-\theta\right), Nt\phi'+Nb\theta'=0 \quad at \quad \eta=0\\ &f'=0,\ g'=0, \theta=0, \phi=0 \qquad\qquad\qquad\qquad\qquad\quad at \quad \eta=\infty \end{aligned} \tag{14}$$

Where Thermophoresis $Nt=\frac{D_T\left(T_w-T_\infty\right)}{\upsilon T_\infty}$, Brownian motion $Nb=\frac{D_B\left(T_w-T_\infty\right)}{\upsilon}$, Prandtl number $\mathrm{Pr}=\frac{\upsilon}{\alpha}$, Magnetic field $M=\frac{\sigma B_0^2}{a\rho}$, Schmidt number $Sc=\frac{\upsilon}{D_m}$. Modified Eckert number $Ec_m=\frac{Ec_x}{Ec_y}$. The interested quantities are friction coefficients in the x and y directions which are connected by two physical parameters C_{fx} and C_{fy}, the local Nusselt and Sherwood numbers are defined by:

$$C_{fx}=\frac{\tau_{wx}}{\rho u_e^2},\quad C_{fy}=\frac{\tau_{wy}}{\rho v_e^2}, Nu_x=\frac{xq_w}{k\left(T_w-T_\infty\right)}, Sh_x=\frac{xs_w}{D_B\left(C_w-C_\infty\right)} \tag{15}$$

Where $\tau_{wx}=\mu\left(1+\frac{1}{\beta}\right)\frac{\partial u}{\partial z}\Big|_{z=0}$ and $\tau_{wy}=\mu\left(1+\frac{1}{\beta}\right)\frac{\partial v}{\partial z}\Big|_{z=0}$, the surface shear stress along the x and y directions, respectively, $q_w=-k\frac{\partial T}{\partial z}\Big|_{z=0}$ the surface heat flux, and $s_w=-D_B\frac{\partial C}{\partial z}\Big|_{z=0}$ is the surface mass flux.

Using Eq. (9), we obtain

$$\begin{aligned} &\left[\mathrm{Re}_x\right]^{\frac{1}{2}}C_{fx}=\left(1+\frac{1}{\beta}\right)f''(0), \left(\frac{x}{y}\right)C_{fy}\left[\mathrm{Re}_x\right]^{\frac{1}{2}}=c\left(1+\frac{1}{\beta}\right)g''(0),\\ &\left[\mathrm{Re}_x\right]^{\frac{-1}{2}}Nu_x=-\theta'(0), \left[\mathrm{Re}_x\right]^{\frac{-1}{2}}Sh_x=-\phi'(0), \mathrm{Re}_x=\frac{u_e x}{\upsilon} \end{aligned} \tag{16}$$

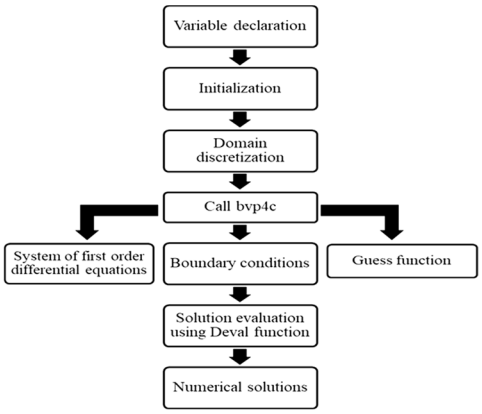

Figure 2. Numerical method Flowchart

3. NUMERICAL METHOD

To effectively solve the given set of nonlinear differential equations (10), (11), (12), (13) and boundary conditions (14), the linearity technique can be used to convert them into first-order ODEs. This will enable us to simplify the problem and solve it more efficiently, leading us towards a constructive solution as follows.

$$y_1 = f, y_2 = f', y_3 = f'', y_4 = g, y_5 = g', y_6 = g'', y_7 = \theta, y_8 = \theta', y_9 = \phi, y_{10} = \phi' \tag{17}$$

$$y_1' = y_2$$

$$y_2' = y_3$$

$$y_3' = \frac{-\left(\left(y_1 + cy_4\right)y_3 - \left(y_2\right)^2 + 1 - M\left(y_2 - 1\right) - \lambda\left(y_2 - 1\right)\right)}{1 + \frac{1}{\beta}}$$

$$y_4' = y_5$$

$$y_5' = y_6$$

$$y_6' = \frac{-\left(\left(y_1 + cy_4\right)y_6 - c\left(y_5\right)^2 + c - M\left(y_5 - 1\right) - \lambda\left(y_5 - 1\right)\right)}{1 + \frac{1}{\beta}}$$

$$y_7' = y_8$$

$$y_8' = \frac{-\Pr\left(\left(y_1 + cy_4\right)y_8 + Nb\, y_8 y_{10} + Nt\left(y_8\right)^2\right)}{1 + \frac{4}{3}Rd}$$

$$y_9' = y_{10}$$

$$y_{10}' = -\left(Sc\left(y_1 + cy_4\right)y_{10} + \frac{Nt}{Nb}\left(y_8'\right) - Sc\ \sigma\left(1 + \delta y_7\right)^n\ e^{\left(\frac{-E}{1+\delta y_7}\right)}y_9\right)$$

where the initial conditions

$$\begin{aligned} &y_1(0) = 0, y_2(0) = 0, y_3(0) = I_1, y_4(0) = 0, y_5(0) = 0, y_6(0) = I_2, \\ &y_7(0) = I_3, y_8(0) + Bi\left(1 - y_7(0)\right) = 0, y_9(0) = I_4, Nt\, y_{10}(0) + Nb\, y_8(0) = 0 \end{aligned} \tag{18}$$

Arbitrary parameters, denoted by I_1, I_2, I_3, I_4, will be determined to solve the system of equations given in Eq. (17) along with the initial conditions listed in (18). The MATLAB program is used in combination with the shooting method and the fourthorder Runge-Kutta method to solve the system. The obtaining the results in a sequence of steps, these are well present in Fig.2. The program ensures that the error is minimized and the final conditions are met.

$$y_1(\infty) = 0,\ y_4(\infty) = 0,\ y_7(\infty) = 0, y_9(\infty) = 0\,.$$

In order to verify the validity of our code, we conducted a comparison of the skin friction coefficient results obtained for Reynolds number of pure water with those previously reported by Wang [24], Ishak et al. [6] and Ahmed et al. [1]. After conducting the analysis, we observed that our results were in better agreement with those reported in Table 1. This comparison was an essential step in ensuring that our code was accurately simulating the physical phenomenon being studied.

Table 1. Comparison of various values of skin friction, for regular fluid (water) and Pr = 0.7

Re	Wang [24]	Ishak et al. [6]	Ahmed et al. [1]	Present
2	−1.59390	−1.5941	−1.59444	−1.6061299
5	−2.41745	−2.4175	−2.41798	−2.420235
10	−3.34445	−3.3445	−3.34511	−3.345029

4. RESULTS AND DISCUSSION

The presented data includes the numerical outcomes of fluid velocity, thermal distribution, and nanoparticle distribution. ***Worth note that the results are indicates Newtonian fluid – Dashed lines and Non-Newtonian Casson fluid – Soid line***. The graphs and tables provided an analysis of the impact of different parameters, such as the Brownian motion parameter ***Nb***, magnetic parameter ***M***, porous medium parameter ***λ***, thermal radiation parameter ***Rd***, Gradient of

streamline parameter ***c***, Casson fluid parameter ***β***, thermophoresis parameter ***Nt***, chemical reaction parameter ***σ***, thermal biot number ***Bi***, activation energy parameter ***E***at a constant value.

In **Fig. 3-20**, the impacts of different parameters on streamwise velocity profiles $f'(\eta)$ and $g'(\eta)$ are illustrated. Specifically, the influence of magnetic parameter M, which measures the magnetic field strength in a porous medium, is shown. Additionally, the impact of porous permeability parameter λ, which characterizes the ability of a porous medium to transmit fluid, is depicted. Finally, the effect of Gradient of streamline parameter c, which relates to the change in streamlines with respect to distance in the direction of flow, is also demonstrated. Overall, these parameters play a major role in determining the behavior of fluid flow.

The comparative analysis of velocity profiles for Newtonian and Casson fluid flows over sinusoidal cylinder with the influenced by magnetic parameter M have been presented in the **Fig 3**. As the magnetic parameter rises, the velocity profiles are increased and worth noting that the greater velocity profile is observed in Newtonian fluid induced by Lorentz force. The similar mechanism of velocity profiles is noted by the porosity parameter, which is observed from the **Fig 4**. The effect of c on the velocity profiles are depicted in the **Fig. 5.**

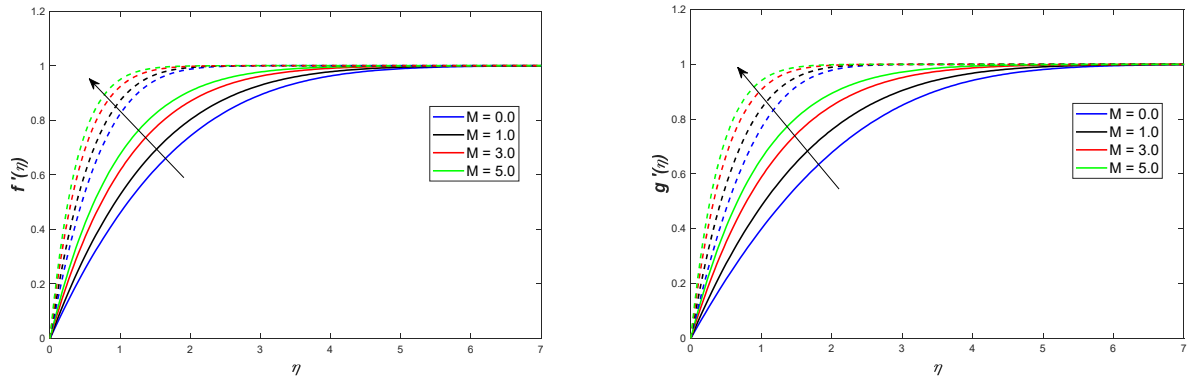

Figure 3. Variation in velocity due to M

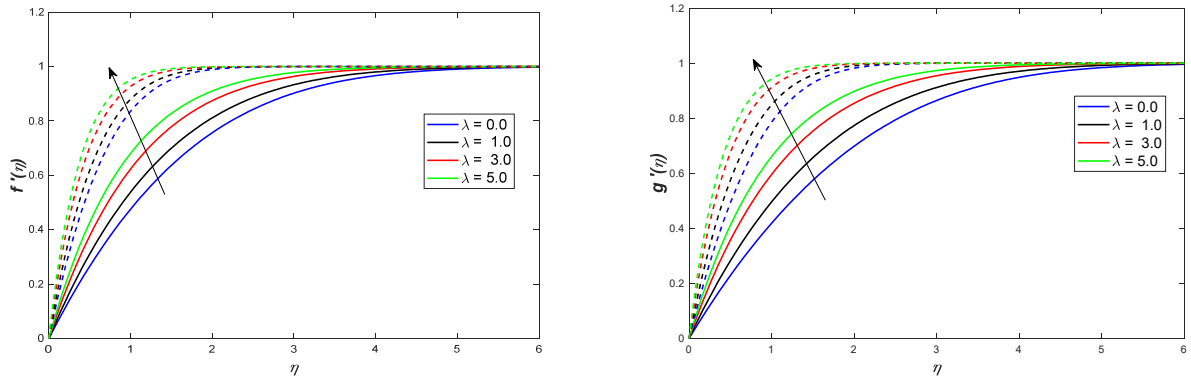

Figure 4. Variation in velocity due to λ

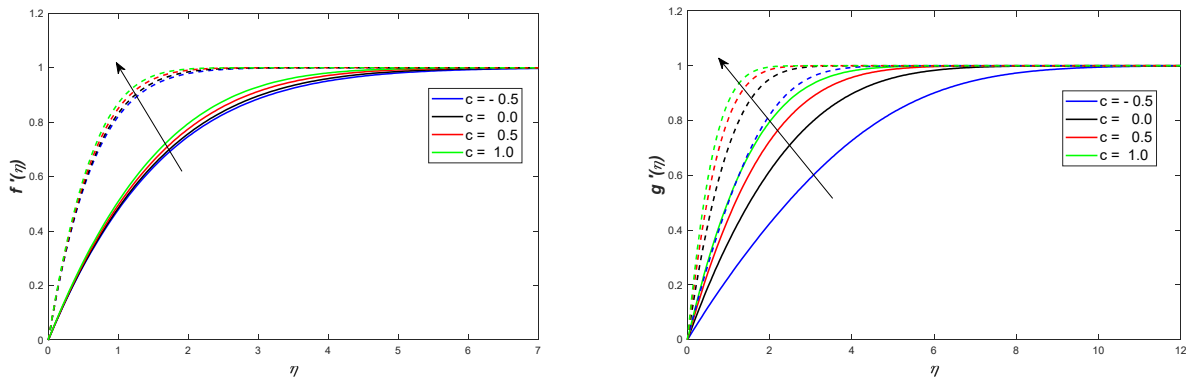

Figure 5. Variation in velocity due to c

The geometry of saddle/nodal stagnation point c plays a crucial role of velocity profiles. The significant impact is observed on the fluid flow velocity profiles is observed with various values of saddle/nodal stagnation point c. majorly

we examine saddle stagnation point, nodal stagnation points and stagnation point. Maximal velocity profile is notice at nodal stagnation points; minimum velocity profile is observed at saddle stagnation point in both velocity profiles.

Figs. 6-12 presents the effect of magnetic parameter M, porosity parameter λ, Nodal/Saddle point c, thermal radiation Rd, thermophoresis Nt, Brownian motion Nb and Biot number Bi, on temperature profile. **Fig. 6 and 7** displays the effect of magnetic parameter and porosity parameter on temperature profiles respectively. The temperature profile decreases in both the fluids when increasing of the magnetic field and porosity. This mechanism is happened due to Lorentz force and the Darcian body force is inversely proportional to the medium. The significant impact is observed on the temperature profiles is observed with various values of nodal/saddle stagnation point c.

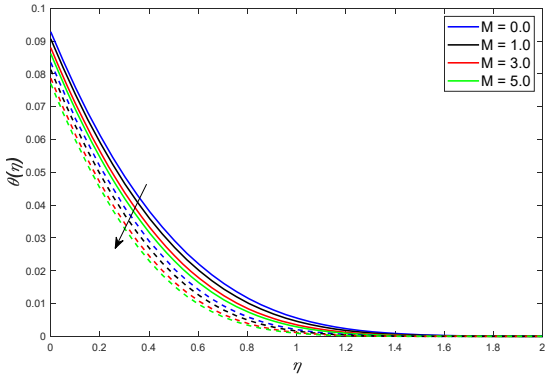

Figure 6. Variation in Temperature due to M

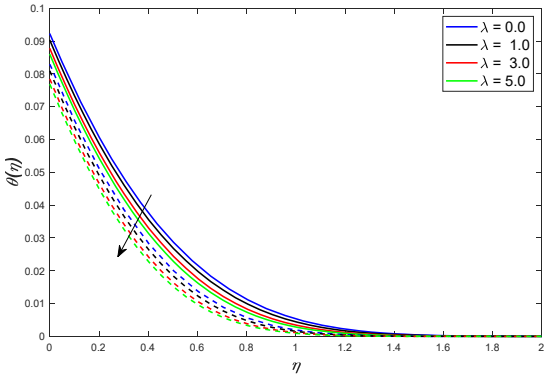

Figure 7. Variation in Temperature due to λ

The thermal distribution reduces with the increasing of the nodal/saddle stagnation point c, is observed in the **Fig. 8**. Thermophoresis ***Nt*** and Brownian motion parameter ***Nb*** impact on temperature profile is depicted in the **Fig. 9 and 10**.

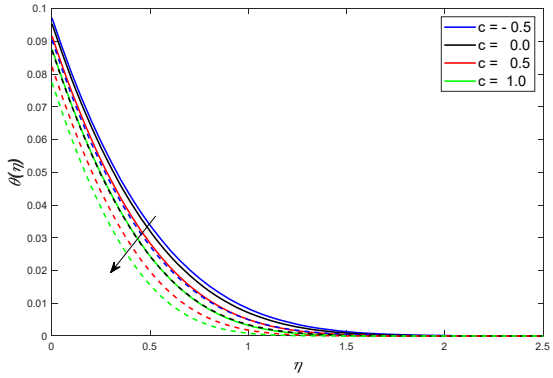

Figure 8. Variation in Temperature due to c

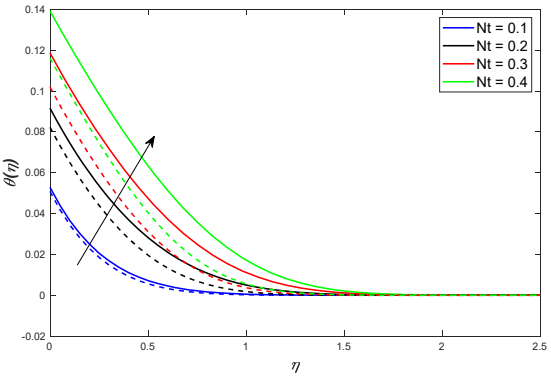

Figure 9. Variation in Temperature due to Nt

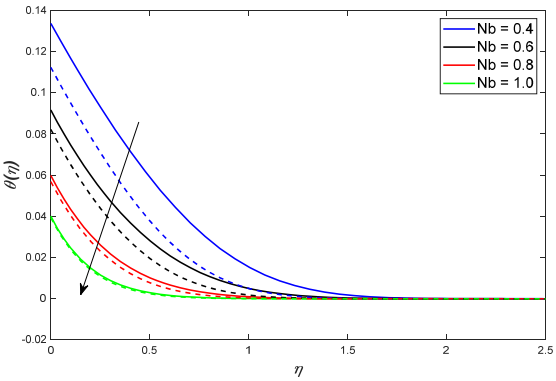

Figure 10. Variation in Temperature due to Nb

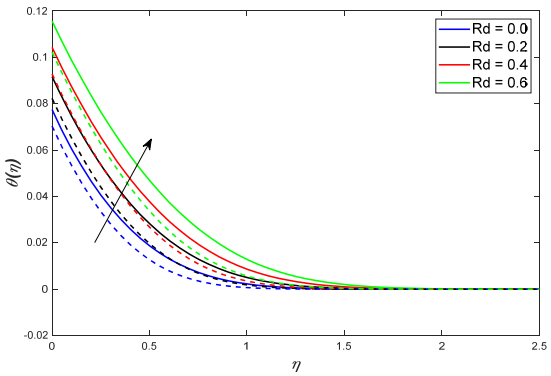

Figure 11. Variation in Temperature due to Rd

Thermophoresis is a fascinating phenomenon that takes place in fluid-particle mixtures. It results from uneven temperature distribution, which leads to the displacement of nanoparticles towards the colder region. This process is driven by thermophoretic forces that cause a non-uniform distribution of particles. To put it simply, thermophoresis is like a tiny invisible hand that pushes particles towards the cold region and causes them to accumulate there. Additionally, the thermophoresis increases as the fluid's temperature increases. Brownian motion is observed in the movement of particles suspended in a fluid. This random movement is caused by the collision of fluid molecules with the particles. The speed

of Brownian motion depends on the particle's size and the fluid's temperature. Larger nanoparticles experience slower Brownian motion, while smaller ones move faster. Additionally, the nanoparticles' Brownian motion increases as the fluid's temperature decreases. The effect of thermal radiation on temperature profile is depicted in the **Fig. 11**.

When thermal radiation is present, it can raise the temperature profile of a fluid. This happens because the thermal radiation parameter helps improve the fluid's thermal conditions, which can lead to more fluid being present in the boundary layer. As a result, the velocity of the fluid may increase.The effect of Biot number Bi on the temperature profile is seen in **Fig. 12**.

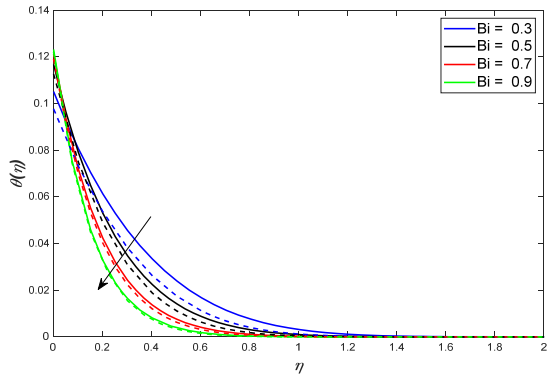

Figure 12. Variation in Temperature due to Bi

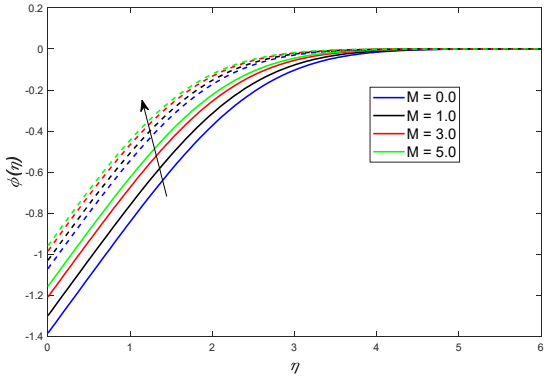

Figure 13. Variation in Temperature due to M

The Biot number is a proper dimensionless quantity when performing heat transfer calculations. It measures the relative resistance to heat transfer due to conduction inside a body versus convection at the body's surface. The temperature profiles reduce with the increasing of Biot number values is observed.

Figs. 13-20 presents the impact of magnetic parameter M, porosity parameter λ, Nodal/Saddle point c, Brownian motion Nb, thermophoresis Nt, Biot number Bi, chemical reaction parameter σ and Activation parameter E on concentration profile. The concentration profile enhancement is observed with the magnetic parameter M, porosity parameter λ, Nodal/Saddle point c, and thermophoresis Nt, when increasing of these parameters the significant increment is notice, which are shown in **Figs. 13-16.** In addition**,** the Casson nanofluid concentration profile is diminishes with incremental values of Nb, Bi, σ, the great observation from the **Figs.17-19** the Brownian motion Nb, Biot number Bi, chemical reaction parameter σ are deaccelerates the concentration profile while the opposite mechanism is found with the Activation parameter E seen in **Fig. 20**.

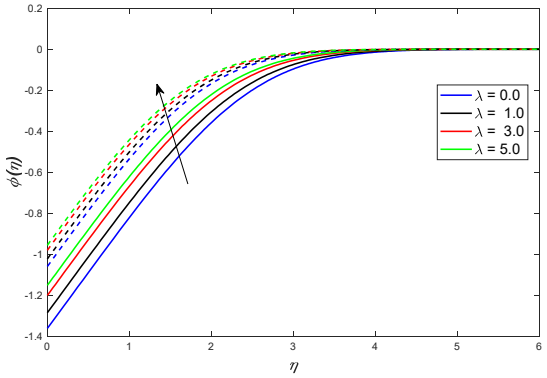

Figure 14. Variation in concentration due to λ

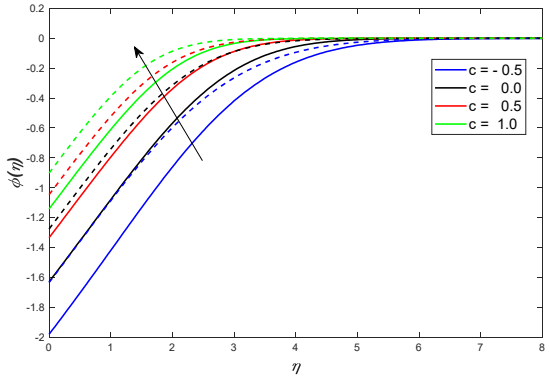

Figure 15. Variation in concentration due to c

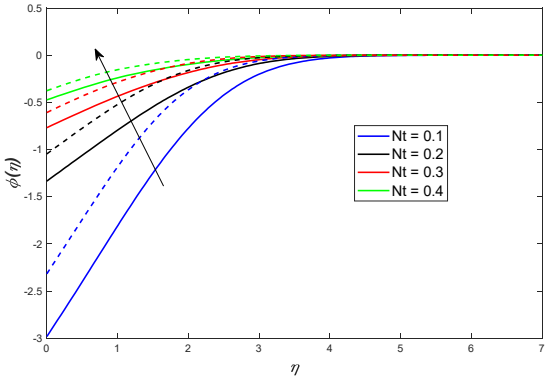

Figure 16. Variation in concentration due to Nt

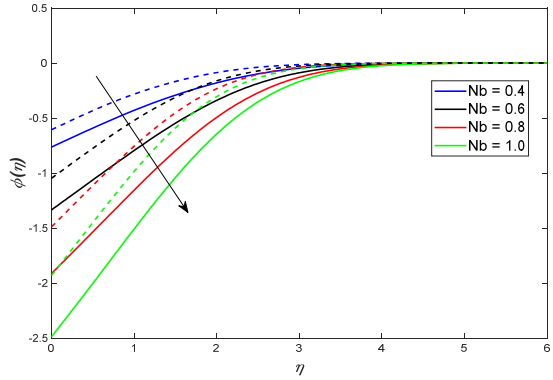

Figure 17. Variation in concentration due to Nb

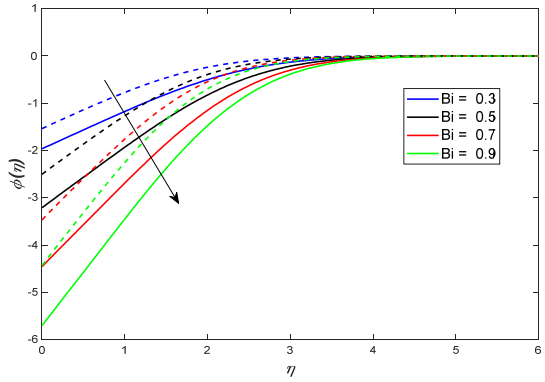

Figure 18. Variation in concentration due to Bi

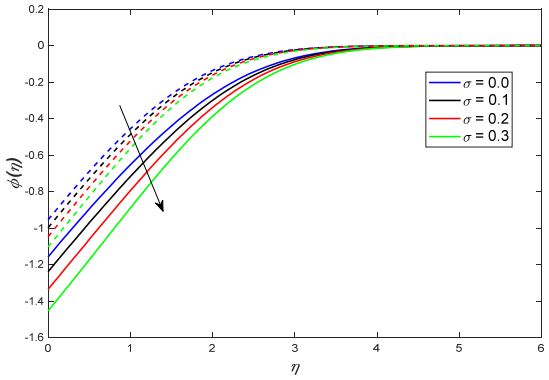

Figure 19. Variation in concentration due toσ

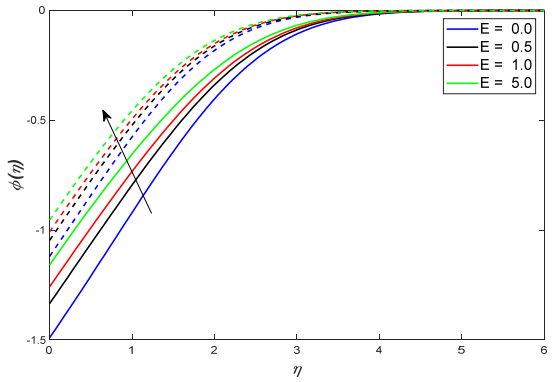

Figure 20. Variation in concentration due to E

The tables provide comprehensive insights into the dynamics of skin friction, Nusselt number and Sherwood number variations, presented in Tables 2, 3, and 4, respectively.

Table 2. Cf_x and Cf_y for various values

c	M	λ	Cf_x		Cf_y	
			β = ∞	β = 0.2	β = ∞	β = 0.2
-0.5			1.5056	0.6146	1.5056	0.6146
0.0			1.5212	0.6210	1.5212	0.6210
0.5			1.5495	0.6326	1.5495	0.6326
1.0			1.5841	0.6467	1.5841	0.6467
	0.0		1.3796	0.5632	1.3796	0.5632
	1.0		1.7027	0.6951	1.7027	0.6951
	3.0		2.2123	0.9032	2.2123	0.9032
	5.0		2.6252	1.0717	2.6252	1.0717
		0.0	1.4500	0.5919	1.4500	0.5919
		1.0	1.7602	0.7186	1.7602	0.7186
		30.	2.2570	0.9214	2.2570	0.9214
		5.0	2.6630	1.0871	2.6630	1.0871

Table 3. Nu values for different emerging parameter values

Bi	Rd	M	Nb	Nt	c	Nu	
						β = ∞	β = 0.2
0.3						0.1238	0.1332
0.5						0.1428	0.1479
0.7						0.1508	0.1534
0.9						0.1546	0.1560
	0.0					0.0703	0.0774
	0.2					0.1042	0.1161
	0.4					0.1423	0.1599
	0.6					0.1839	0.2081
		0.0				0.1057	0.1176
		1.0				0.1030	0.1149
		3.0				0.0997	0.1115
		5.0				0.0976	0.1092

Bi	Rd	M	Nb	Nt	c	Nu	
						$\beta = \infty$	$\beta = 0.2$
			0.4			0.1424	0.1694
			0.6			0.1042	0.1161
			0.8			0.0721	0.0759
			1.0			0.0498	0.0509
				0.1		0.0643	0.0670
				0.2		0.1042	0.1161
				0.3		0.1292	0.1504
				0.4		0.1472	0.1764
					-0.5	0.1146	0.1230
					0.0	0.1106	0.1208
					0.5	0.1042	0.1161
					1.0	0.0981	0.1109

Table 4. Sh values for different emerging parameter values

c	M	Nb	Nt	Bi	σ	E	Sh	
							$\beta = \infty$	$\beta = 0.2$
-0.5							1.6335	1.9807
0.0							1.2756	1.6293
0.5							1.0463	1.3343
1.0							0.9018	1.1418
	0.0						1.0695	1.3828
	1.0						1.0285	1.2977
	3.0						0.9838	1.2071
	5.0						0.9582	1.1556
		0.4					0.6059	0.7632
		0.6					1.0463	1.3343
		0.8					1.4884	1.9125
		1.0					1.9302	2.4872
			0.1				2.3170	2.9825
			0.2				1.0463	1.3343
			0.3				0.6081	0.7686
			0.4				0.3763	0.4732
				0.3			1.5364	1.9625
				0.5			2.5039	3.2102
				0.7			3.4685	4.4576
				0.9			2.5039	3.2102
					0.0		0.9535	1.1570
					1.0		0.9971	1.2377
					2.0		1.0463	1.3343
					3.0		1.1022	1.4523
						0.0	1.1190	1.4895
						0.5	1.0463	1.3343
						1.0	1.0074	1.2576
						5.0	0.9544	1.1588

These parameters offer crucial physical understanding of the heat and mass transfer processes within the system. Notably, as the unsteadiness parameter increases, both skin friction coefficients and local Nusselt numbers show a consistent uptrend. This indicates that higher levels of unsteadiness correspond to increased frictional forces and enhanced convective heat transfer rates from the surface to the fluid. However, an intriguing observation emerges when examining local Sherwood number. At a critical value of the unsteadiness parameter, particularly when thermophoresis effects come into play, a minimum local Sherwood number is noted. This phenomenon suggests a nuanced interplay between unsteadiness and thermophoresis, where certain conditions may optimize mass transfer rates. Moreover, the analysis underscores the significance of thermophoresis effects on heat transfer. It is evident that the highest heat transfer rates occur under conditions where thermophoresis effects are minimal. Conversely, increasing the thermophoresis parameter leads to a reduction in heat transfer rates, indicating the inhibitory role of thermophoresis on overall heat transfer efficiency. Furthermore, the behavior of the local Nusselt number unveils additional insights. With the rise in the unsteadiness parameter, the local Nusselt number escalates, reflecting the heightened convective heat transfer rates characteristic of more dynamic flow conditions. Notably, peak heat transfer rates are achieved when Brownian motion is minimal or approaches zero, emphasizing the intricate relationship between flow dynamics and particle behavior. Finally, the occurrence of negative local Nusselt numbers for certain unsteadiness parameter values is particularly intriguing. Such instances signify a reversal in the heat transfer direction, indicating heat transfer from the nanofluid to the body. This phenomenon underscores the complex interplay of various parameters in determining the directionality and efficiency of

heat transfer processes within the system, highlighting the need for a comprehensive understanding of fluid dynamics and transport phenomena.

5. CONCLUSIONS

In summary, our investigation delved into a transient three-dimensional boundary layer scenario surrounding the flow of magnetohydrodynamic (MHD) Casson polymeric nanofluid around a wavy circular porous cylinder. Incorporating considerations of thermal radiation and activation energy, we emphasized the nonlinear aspects of chemical reaction in the energy equation and utilized convective Nield boundary conditions for a comprehensive analysis. By transforming the boundary layer equations into a self-similar form, we enabled numerical solutions. Notably, we observed the expansion of the velocity field with a certain indicative parameter and its flattening in the presence of an external magnetic field. The impact of thermal conditions on heating and cooling processes proved significant, emphasizing the need for minimization, particularly in air conditioning systems. Furthermore, as the porous parameter increased, we noted improvements in the thermal boundary layer and weakening in the concentration boundary layer. Our findings revealed that the Nusselt number increased with advancements in the thermal radiation parameter and the Sc number within the thermal boundary layer regime. Additionally, we observed a proportional rise in the Nusselt number with increasing activation energy and a decrease in wall mass. Moreover, variations in the nodal/saddle point parameter resulted in changes in the skin-friction coefficients. Finally, we found that the Nusselt number decreased with higher *Bi* values but increased with rising Brownian parameters, and increasing activation energy led to a decrease in the Sherwood number. These insights offer valuable contributions to understanding the complex dynamics of boundary layer phenomena in fluid mechanics and thermal transport processes.

Declaration of Competing Interest

The authors declare that they have no known competing financial interests or personal relationships that could have appeared to influence the work reported in this paper.

Conflict of interest statement

The authors did not disclose any possible conflicts of interest.

Data availability statement

There are no data related to the text.

CRediT authorship contribution statement

P. Venkata Subrahmanyam: Writing – review & editing, Writing – original draft, Visualization, Validation, Methodology, Investigation, Conceptualization. G. Kathyayani: Supervision. G. Venkata Ramudu: Supervision.

Funding Declaration

This research did not receive any specific grant from funding agencies in the public, commercial, or not-for-profit sectors.

ORCID

Gandrakota Kathyayani, https://orcid.org/0000-0002-1019-7033
Gattu Venkata Ramudu, https://orcid.org/0009-0001-0253-6613
K. Venkatadri, https://orcid.org/0000-0001-9248-6180

REFERENCES

[1] S.E. Ahmed, A.K. Hussein, H.A. Mohammed, and S. Sivasankaran, "Boundary layer flow and heat transfer due to permeable stretching tube in the presence of heat source/sink utilizing nanofluids," Applied Mathematics and Computation, **238**, 149-162 (2014). https://doi.org/10.1016/j.amc.2014.03.106

[2] D. Tripathi, A. Sharma, and O.A. Beg, "Joule heating and buoyancy effects in electro-osmotic peristaltic transport of aqueous nanofluids through a microchannel with complex wave propagation," Adv. Powder Technol. **29**, 639–653 (2018). https://doi.org/10.1016/j.apt.2017.12.009

[3] F. Alwawi, H. Alkasasbeh, A. Rashad, and R. Idris, "Heat transfer analysis of ethylene glycol-based casson nanofluid around a horizontal circular cylinder with MHD effect," Proceedings of the Institution of Mechanical Engineers Part C Journal of Mechanical Engineering Science, **234**(13), 2569-2580(2020). https://doi.org/10.1177/0954406220908624

[4] F. Bosli, A. Suhaimi, S. Ishak, M. Ilias, A. Rahim, and A. Ahmad, "Investigation of nanoparticles shape effects on aligned MHD Casson nanofluid flow and heat transfer with convective boundary condition," Journal of Advanced Research in Fluid Mechanics and Thermal Sciences, **91**(1), 155-171(2022). https://doi.org/10.37934/arfmts.91.1.155171

[5] G. Narender, K. Govardhan, and G. Sarma, "Magnetohydrodynamic stagnation point on a casson nanofluid flow over a radially stretching sheet," Beilstein Journal of Nanotechnology, **11**, 1303-1315 (2020). https://doi.org/10.3762/bjnano.11.114

[6] A. Ishak, R. Nazar, and I. Pop, "Uniform suction/blowing effect on flow and heat transfer due to a stretching cylinder," Applied Mathematical Modelling, **32**(10), 2059-2066 (2008). https://doi.org/10.1016/j.apm.2007.06.036

[7] J. Akram, N.S. Akbar, and D. Tripathi, "Numerical simulation of electrokinetically driven peristaltic pumping of silver-water nanofluids in an asymmetricmicro-channel," Can. J. Phys. **68**, 745–763 (2020). https://doi.org/10.1016/j.cjph.2020.10.015

[8] J. Buongiorno, "Convective transport in nanofluids," ASME J. Heat Transfer, **128**, 240–250 (2006). https://doi.org/10.1115/1.2150834

[9] K. Gnanaprasanna, and A. Singh, "A numerical approach of forced convection of casson nanofluid flow over a vertical plate with varying viscosity and thermal conductivity," Heat Transfer, **51**(7), 6782-6800 (2022). https://doi.org/10.1002/htj.22623

[10] G. Kathyayani, and P.V. Subrahmanyam, "Numerical study of MHD Stagnation-Point Flow of Nanofluid Flow Past a 3-D Sinusoidal Cylinder with Thermophoresis and Brownian Motion Effects," in: *Disruptive Technologies in Computing and*

Communication Systems – Conference Proceedings, (Taylor & Francis Group, London, 2024), pp. 408-406, https://doi.org/10.1201/9781032665535-66
[11] G. Kathyayani, and R.L. Devi, "Effect of induced magnetic field and Linear / non-linear vertical stretching sheet on mixed convection Jeffrey fluid near a Stagnation-Point flow through a Porous medium with suction or injection," J. Phys.: Conf. Ser. **1597**, 012003 (2020). https://doi.org/10.1088/1742-6596/1597/1/012003
[12] L. Panigrahi, J. Panda, K. Swain, and G. Dash, "Heat and mass transfer of mhdcasson nanofluid flow through a porous medium past a stretching sheet with newtonian heating and chemical reaction," Karbala International Journal of Modern Science, **6**(3), (2020). https://doi.org/10.33640/2405-609x.1740
[13] M. Baig, G. Chen, and C. Tso, "The thermal performance analysis of an al2o3-water nanofluid flow in a composite microchannel," Nanomaterials, **12**(21), 3821 (2022). https://doi.org/10.3390/nano12213821
[14] M.K. Nayak, "MHD 3D flow and heat transfer analysis of nanofluids by shrinking surface inspired by thermal radiation and viscous dissipation," Int. J. Mech. Sci. **124**, 185–193 (2017). https://doi.org/10.1016/j.ijmecsci.2017.03.014
[15] M.K. Nayak, N.S. Akbar, D. Tripathi, and V.S. Pandey, "Three dimensional MHD flow of nanofluid over an exponential porous stretching sheet with convective boundary conditions," Therm. Sci. Eng. Prog. **3**, 133–140 (2017). https://doi.org/10.1016/j.tsep.2017.07.006
[16] M.K. Nayak, N.S. Akbar, D. Tripathi, Z.H. Khan, and V.S. Pandey, "MHD 3D free convective flow of nanofluid over an exponentially stretching sheet with chemical reaction," Adv. Powder Technol. **28**, 2159–2166 (2017). https://doi.org/10.1016/j.apt.2017.05.022
[17] M. Senapati, K. Swain, and S. Parida, "Numerical analysis of three-dimensional mhd flow of casson nanofluid past an exponentially stretching sheet," Karbala International Journal of Modern Science, **6**(1), (2020). https://doi.org/10.33640/2405-609x.1462
[18] N.A. Halim, R.U. Haq, and N.F.M. Noor, "Active and passive controls of nanoparticles in Maxwell stagnation point flow over a slipped stretched surface," Meccanica, **52**, 1527–1539 (2017). https://doi.org/10.1007/s11012-016-0517-9
[19] N. Thamaraikannan, S. Karthikeyan, D. Chaudhary, and S. Kayikci, "Analytical investigation of magnetohydrodynamic non-newtonian type casson nanofluid flow past a porous channel with periodic body acceleration," Complexity, **2021**, 1-17 (2021). https://doi.org/10.1155/2021/7792422
[20] P. Rana, N. Shukla, O.A. Bég, *et al*., "Lie Group Analysis of Nanofluid Slip Flow with Stefan Blowing Effect via Modified Buongiorno's Model: Entropy Generation Analysis," Differ. Equ. Dyn. Syst. **29**, 193–210 (2021). https://doi.org/10.1007/s12591-019-00456-0
[21] S. Han, L. Zheng, C. Li, and X. Zhang, "Coupled flow and heat transfer in viscoelastic fluid with Cattaneo-Christov heat flux model," Appl. Math. Lett. **38**, 87–93 (2014). https://doi.org/10.1016/j.aml.2014.07.013
[22] V.K. Narla, D. Tripathi, and O.A. Beg, "Electro-osmotic nanofluid flow in a curved microchannel," Can. J. Phys. **67**, 544-558 (2020). https://doi.org/10.1016/j.cjph.2020.08.010
[23] V. Tibullo, and V. Zampoli, "A uniqueness result for the Cattaneo-Christov heat conduction model applied to incompressible fluids," Mech. Res. Commun. **38**, 77–79 (2011). https://doi.org/10.1016/j.mechrescom.2010.10.008
[24] C.Y. Wang, "Fluid flow due to a stretching cylinder," The Physics of fluids, **31**(3), 466-468 (1988). https://doi.org/10.1063/1.866827
[25] Y. Wang, K. Yang, Z. Zhang, W. Qi, and J. Yang, "Natural convection heat and moisture transfer with thermal radiation in a cavity partially filled with hygroscopic porous medium," Drying Technology, **34**(3), 275-286 (2015). https://doi.org/10.1080/07373937.2015.1047953

ТОЧКА СТАГНАЦІЇ МГД-ПОТОКІВ ПОЛІМЕРНОЇ НАНОРІДИНИ КАССОНА У НАПРЯМКУ ДО ХВИЛЯСТОГО КРУГОВОГО ЦИЛІНДРУ, НАСИЧЕНОГО ПОРИСТИМ СЕРЕДОВИЩЕМ В УМОВАХ КОНВЕКТИВНОГО ПОЛЯ І ТЕПЛОВОГО ВИПРОМІНЮВАННЯ

П. Венката Субрахманьям[a], Гандракота Катьяяні[a], Гатту Венката Рамуду[a], К. Венкатадрі[b]
[a]Кафедра прикладної математики, Університет Йогі Вемана, Кадапа, А.П., Індія
[b]Кафедра математики, Університет Мохана Бабу (колишній інженерний коледж Шрі Відьянікетан), Тірупаті А.Р.-517 102, Індія

У цьому дослідженні проводиться ретельне числове дослідження з використанням методу bvp4c для вивчення потоку магнітогідродинамічної (МГД) полімерної нанорідини Кассона навколо хвилястого круглого пористого циліндра в точці застою. У ньому враховується енергія активації та теплове випромінювання, що підкреслює значний вплив теплового випромінювання на потік рідини, концентрацію та профілі температури. Вплив теплового випромінювання в рівнянні енергії ретельно розглянуто разом з конвективними граничними умовами Нільда, що дозволяє провести комплексний аналіз. Вводячи безрозмірні змінні, дослідження перетворює диференціальне рівняння з частинними похідними на звичайні рівняння, що полегшує застосування схеми стрільби для наближення розв'язку. Ретельно досліджені результати пропонують детальне розуміння профілів температури, швидкості та масової концентрації, підкреслюючи глибокий вплив теплового випромінювання на ці параметри. Крім того, надається комплексне графічне представлення кожного інженерного параметра, що пропонує тонке розуміння складних фізичних явищ, що беруть участь, з особливою увагою до впливу теплового випромінювання.

Ключові слова: *потік у точці застою; теплове випромінювання; полімерна нанорідина Кассона; метод bvp4c; магнітогідродинаміка (МГД)*